ELSEVIER

Journal of Nuclear Materials 297 (2001) 77–88

journal of nuclear materials

www.elsevier.com/locate/jnucmat

Characterisation of pre-transition oxides on Zircaloys

M. Oskarsson [a], E. Ahlberg [b], U. Andersson [b], K. Pettersson [a,*]

[a] *Department of Materials Science and Engineering, Royal Institute of Technology, SE 10044 Stockholm, Sweden*
[b] *Department of Chemistry, Göteborg University, SE 41296 Göteborg, Sweden*

Received 13 October 2000; accepted 4 April 2001

Abstract

The aim of this study was to evaluate the possibility of predicting post-transition oxidation behaviour by studying the properties of pre-transition oxides. Five different zirconium alloys have been tested in autoclave at two different temperatures, 288°C and 360°C. Cross-sectional transmission electron microscopy (TEM) showed that a significant difference in morphology is obtained for the two test temperatures, while the alloy composition was found to have no influence. At the lower test temperature the oxide consists of a mixture of columnar and equiaxed grains, while at the higher temperature mainly columnar grains are observed and the size of these grains is a factor 3–4 longer. Tetragonal oxide phase was mainly detected by selected area diffraction in the thicker oxide layers, while the amount of the tetragonal phase in the thermally formed oxides is too low to be detected by X-ray diffraction. Thus, the tetragonal phase is probably stabilised by other factors than the compressive stress. The impedance measurement shows that the thinnest oxide layers are compact, irrespective of the alloy composition and thermal or anodic oxide growth. For the thicker oxides, a porous outer layer is developed. There is a main difference in the morphology between thermal and anodic oxide layers of the same size, i.e., the anodically formed oxide layer has only equiaxed grains present. Based on the result obtained in this investigation, no prediction of the post-transition oxidation can be made.

1. Introduction

It is well known that the pre-transition oxidation is largely independent of the alloy composition and the environment. The purpose of the present work was therefore to look for differences in microstructure (morphology, pores and cracks) of pre-transition oxides, that can predict the post-transition behaviour.

Two different test temperatures were chosen, the higher temperature is used in autoclave testing of post-transition behaviour and the lower is the reactor temperature. Four different Zircaloy-2 and one Zircaloy-4 alloys were oxidised in an autoclave to produce thin oxide layers. After oxidation the samples were investigated by X-ray diffraction, cross-sectional transmission electron microscopy (TEM) and electrochemical impedance spectroscopy (EIS).

Zirconium has a very high affinity for oxygen and even at room temperature a thin oxide layer is formed. This air-formed film is characterised by small oxide grains, due to the high nucleation rate, and the layer is 2–5 nm thick [1,2]. The growth of the oxide layer takes place at the metal/oxide interface [3,4] and the initially formed oxide is characterised by small oxide grains, ~5 nm, due to nucleation at many sites [5]. During pre-transition oxidation the diffusion of oxygen ions through the existing oxide layer is the rate limiting process. This process is thermally activated and a higher temperature will of course result in a higher diffusion rate. The oxygen diffusion takes place mainly in the grain boundaries; the rate for grain boundary diffusion is 10^4 higher in oxygen [6] and 10^8 in water vapour [7] compared to bulk diffusion. The initial growth of the oxide is governed by a parabolic growth behaviour, a natural consequence of oxygen diffusion through the growing layer being the rate controlling process. However, the expo-

* Corresponding author. Tel.: +46-8 790 9194; fax: +46-8 207 681.
E-mail address: kjellp@met.kth.se (K. Pettersson).

0022-3115/01/$ - see front matter
PII: S0022-3115(01)00580-3

nent 1/3 rather than 1/2 on the time indicates that the grain structure coarsens with growth so that the available grain boundary area for diffusion decreases with growth [5]. At a certain thickness of the oxide, typically about 2 μm, the growth rate becomes linear with time. This is the so-called transition and for practical purposes the post-transition rate of oxide growth is the most important property of a zirconium alloy. Despite years of research the mechanism behind the transition is still not understood. A common model is to assume that the stresses in the oxide increase causing a purely mechanical failure of the oxide and the oxide film cracks. It has been hypothesised and to some extent confirmed by various characterisation methods that the oxide formed under stress is the tetragonal modification of zirconia. When the stresses are released the tetragonal phase transforms to the monoclinic phase stable at low temperature. The volume change associated with the transformation is believed to induce porosity in the oxide layer. The porosity degrades the protective properties of the oxide and only in a layer close to the metal/oxide interface an undamaged and protective layer remains. This so-called barrier layer is often believed to control the post-transition rate of oxide growth. It is at least conceptually reasonable to assume that the post-transition rate is controlled by factors which either influence the average thickness of the barrier layer or which influence the oxygen transport properties of the layer, or both. Under certain conditions and for certain variants of Zircaloy, for instance when LiOH has been added to the water, an acceleration of the post-transition rate may take place. This may be called a secondary transition.

The properties of the formed oxide layer are potentially influenced by many factors, such as: surface roughness, temperature, environment, second phase particles (SPP), texture of the metal grains and high hydrogen levels in the metal. The complexity of the system indicates that several of these factors co-operate to achieve the specific properties and it is often impossible to decide which of the factors dominates. However, by studying each factor individually a few general statements can be made:

The surface roughness influences the number of nucleation sites; a smoother surface decreases the number of nuclei and the stress distribution. Temperature and environment control the oxygen activity at the outer surface, however the oxidation rate is diffusion controlled.

Second phase particles are believed to affect the crystal structure of the oxide, i.e., monoclinic, tetragonal or cubic phase, and the development of cracks and pores [8,9].

Studies of the oxidation rate on single crystals of van Arkel zirconium, after 40 min in steam at 500°C and 1 atm, have shown variations in weight gain as a function of crystal orientation [10]. Some orientations appear to be more favourable than others.

Corrosion tests on pre-hydrided Zircaloy have shown that high initial hydrogen levels increase the oxidation rate at long exposure times [11], while the pre-transition oxidation rate seems to be unaffected by high initial hydrogen levels. Different mechanisms have been proposed to explain the hydride induced accelerated oxidation behaviour; destruction of the barrier layer by fracture of hydrides at the oxide/metal interface [12], modification of the oxide when it grows on a matrix with high hydrogen levels [13] and higher density of cracks in the oxide formed on massive hydride layers [14]. Pre-transition oxidation of pre-hydrided Zircaloy-2 has shown that the oxidation of massive zirconium hydride resembles the oxidation of zirconium metal. Based on this observation it is suggested that the accelerated oxidation of zirconium alloys cannot be due solely to the presence of a massive hydride layer, but must require a combined effect of, for example interfacial roughness and hydride precipitation [15].

2. Material

The materials used for the present investigation were four Zircaloy-2 variants and one Zircaloy-4, with the chemical compositions given in Table 1.

Zircaloy-2 cladding manufactured by Sandvik AB is available in different modifications, LK-0, LK-1, LK-2, LK-2+ and LK-3. The main difference between these types is the size distribution of SPP. For LK-0, LK-1 and LK-2 the SPP size decreases with increased number [16]. The LK-2+ and LK-3 variants were developed in order to get a better corrosion resistance at high burn-ups. These alloys are characterised by an increased particle size compared to LK-2.

Table 1
Chemical composition

Sample	Sn (%)	Fe (%)	Cr (%)	Ni (%)	Process
Zry-2:A	1.01	0.195	0.095	0.145	LK-2
Zry-2:B	1.335	0.17	0.1	0.05	Zr-2P
Zry-2:C	1.385	0.18	0.105	0.05	LK-3
Zry-2:D	1	0.2	0.1	0.15	Zr-2
Zry-4:A	1.36	0.21	0.095	0.0015	Zr-4

The sample Zry-2:A is an LK-2 type of Zircaloy-2 with a tin content below the ASTM-standard (B 353-85) and with a mean diameter of the second phase particles of 100 nm. The sample Zry-2:B is optimised for PWR conditions, i.e. the tin content is decreased and the mean diameter of the SPPs is 240 nm. The sample Zry-2:C (LK-3) is a standard Zircaloy-2 alloy with a mean diameter of the SPPs of 150 nm. Sample Zry-2:D is a Zircaloy-2 with a tin content lower than what is given in the ASTM-standard. The mean diameter of the SPPs is 310 nm for this sample. Sample Zry-4:A, is a Zircaloy-4 alloy with a composition within the ASTM-standard and a mean diameter of the SPPs of 160 nm. All studied samples were delivered in the form of tubes.

3. Experimental details

The five studied zirconium alloys were oxidised in an autoclave with 14 l volume at 288°C and 72 bar for 20 and 168 h and at 360°C and 186 bar for 96 h. The pressure was chosen so that the corrosion test was performed in liquid water at both temperatures.

One alloy, Zry-2:B, was also tested by anodic oxidation in 0.5 M H_2SO_4 at 100 V and room temperature.

Phase composition was determined by X-ray diffraction using a Siemens 5000 power diffractometer. A grazing angle detector technique was used with an angle of 1° of the incoming beam against the specimen surface. Intensity spectra were recorded between 20° and 70°. A JEOL 2000 EX scanning transmission electron microscope was used to characterise the microstructure of the oxide layers. Cross-sectional thin foils of the oxide layers were produced from the autoclaved samples and the detailed procedure is given elsewhere [15].

A three-electrode cell was used for the impedance experiments in aqueous 0.5 M H_2SO_4. One cm of the autoclaved Zircaloy tubes was used as working electrodes in the impedance measurements. A large platinum gauze was used as the counter electrode and was placed in a concentric position around the working electrode to assure a good current distribution. The potential was measured against a double junction Ag/AgCl reference electrode with 0.5 M H_2SO_4 in the outer compartment. All impedance measurements were carried out at room temperature, in the frequency range 0.01 Hz–100 kHz. The instrumentation used was an EG&G Princeton Applied Research Potentiostat/Galvanostat Model 273A and a Lock in amplifier model 5210.

The impedance data were fitted to equivalent circuits with one, two or three time constants in series, using the Boukamp's fitting program 'Equivalent circuit'. The number of time constants used depends on the complexity of the impedance spectra.

Zirconium oxide is highly insulating and the overall impedance can therefore be attributed to the impedance of the oxide. The oxide behaves like a capacitor in the impedance measurements and the thickness can be calculated by the expression for a parallel plate capacitor,

$$d = \frac{\varepsilon_o \varepsilon_r A}{C}, \tag{1}$$

where ε_o is the dielectric constant of vacuum, ε_r the relative dielectric constant for ZrO_2, A is the geometric surface area, d is the thickness of the oxide layer and C is the capacitance. The impedance data exhibit some frequency dispersion and a constant phase element was used instead of a capacitor. Due to the frequency dispersion the capacitance, and thereby the calculated thickness will vary with frequency. For the rather thin oxide films investigated in the present study, the impedance was corrected for the frequency dispersion according to $|Z|^{1/\alpha}$ and $\Phi \cdot 1/\alpha$, which are valid for rough surfaces [17,18]. Further details about the impedance measurements can be found elsewhere [19].

4. Results

The oxide thickness was estimated by weight gain, TEM and EIS and the results are summarised in Table 2. The oxide thickness measured in TEM is in fairly good agreement with the results from weight gain, while the thickness calculated from the impedance measurements deviates somewhat.

The post-transition oxidation behaviour of the investigated alloys was tested at 360°C and 220 bar in pure water and in water with 70 ppm LiOH added. The results from these tests are presented in Table 3 together

Table 2
Oxide thickness in nm calculated from weight gain/measured in TEM/calculated from EIS

Sample	288°C 20 h	288°C 168 h	360°C 96 h
Zry-2:A	275/250/200	525/500/260 (480)[a]	850/700/930[a]
Zry-2:B	250/150/160	500/650/350	850/800/840
Zry-2:C	175/300/310	400/500/550	775/800/1050
Zry-2:D	300/200/250	550/450/430	900/800/1160
Zry-4:A	200/200/200	400/450/300	750/700/740[a]

[a] After anodisation to 100 V.

Table 3
Autoclave test at 360°C and 220 bar

Sample	Test time (days)	Weight gain (mg/dm^2)	Hydrogen content (ppm)	Environment
Zry-2:A	473	243	1250	70 ppm LiOH
Zry-2:B	200	67	175	H_2O
Zry-2:B	200	664	2750	70 ppm LiOH
Zry-2:C	200	59	145	H_2O
Zry-2:D	200	65	285	H_2O
Zry-2:D	200	205	1150	70 ppm LiOH
Zry-4:A	200	84	160	H_2O
Zry-4:A	353	463	1500	70 ppm LiOH

with the hydrogen content. It can be noted that a high weight gain is also associated with high hydrogen content.

4.1. Zry-2:A

After test for 20 h at 288°C, X-ray diffraction analysis showed the presence of some monoclinic oxide but the main signal is from the metal, see Fig. 1(a). Selected area diffraction (SAD) was used in the TEM analysis to investigate if tetragonal/cubic oxide phase is present in the oxide layers, by studying the (1 0 1) reflection. For this sample some weak spots were detected indicating a small fraction of tetragonal phase present. The morphology of the oxide layer shows a mixture of columnar and equiaxed grains, see Fig. 2(a). The orientation of the columnar grains is perpendicular to the interface, i.e., parallel with the oxide growth direction. A grain is defined as columnar when the observed length is more than twice the width. The oxide grain size has been estimated and the columnar grains are 15–30 × 35–60 nm^2 and the equiaxed grains are 15–30 nm in diameter.

The samples oxidised for 168 h at 288°C have increased oxide thickness and fraction of columnar grains, see Fig. 2(b). X-ray diffraction analysis showed no tetragonal phase, Fig. 1(b), while SAD indicates the presence of tetragonal phase.

The test at 360°C for 96 h gave a thicker oxide layer than in the previous samples. X-ray diffraction analysis showed that the intensity signal from the monoclinic ZrO_2 increases with exposure time and temperature, Fig. 1(c). SAD indicates the presence of tetragonal phase but the content is low since it is not observed in X-ray diffraction. The morphology on this sample is different from the 288°C samples, much longer columnar grains are found (20–50 × 50–150 nm^2), Figs. 2(c) and (d). Also the equiaxed grains are larger (20–40 nm), about 30% more than for the samples tested at 288°C. A few cracks were found in this oxide.

For the sample tested at 288°C for 20 h the film is fairly compact and the thickness determined from the impedance is slightly lower than the estimated thickness from weight gain and TEM, Table 2. For the sample exposed to the same temperature for 168 h a layered oxide is observed. The thickness determined by impedance is considerably lower than that expected from

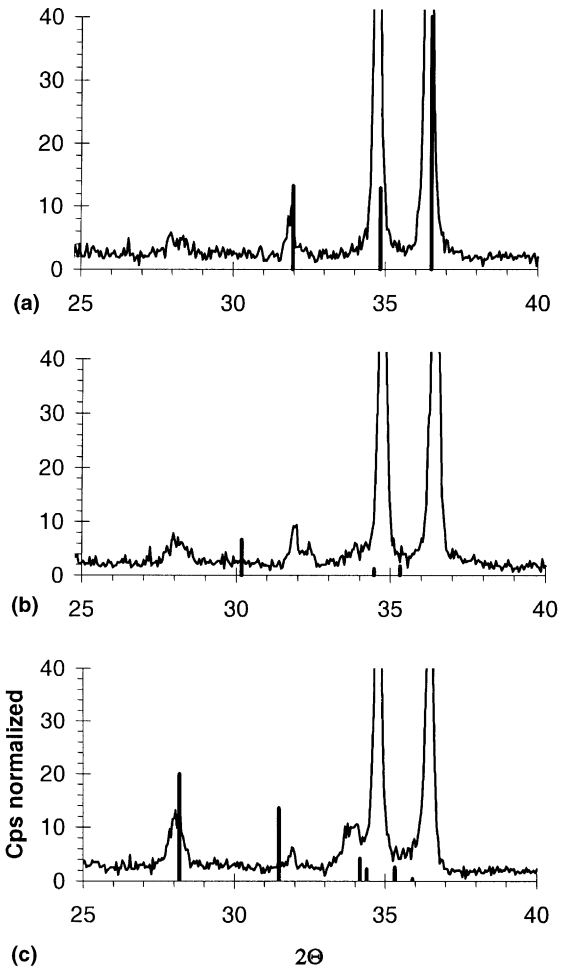

Fig. 1. X-ray diffraction analysis of sample Zry-2:A as a function of exposure time and temperature: (a) 288°C for 20 h; (b) 288°C for 168 h; (c) 360°C for 96 h. The standard reflection for Zr is given in (a), tetragonal ZrO_2 in (b) and monoclinic ZrO_2 in (c).

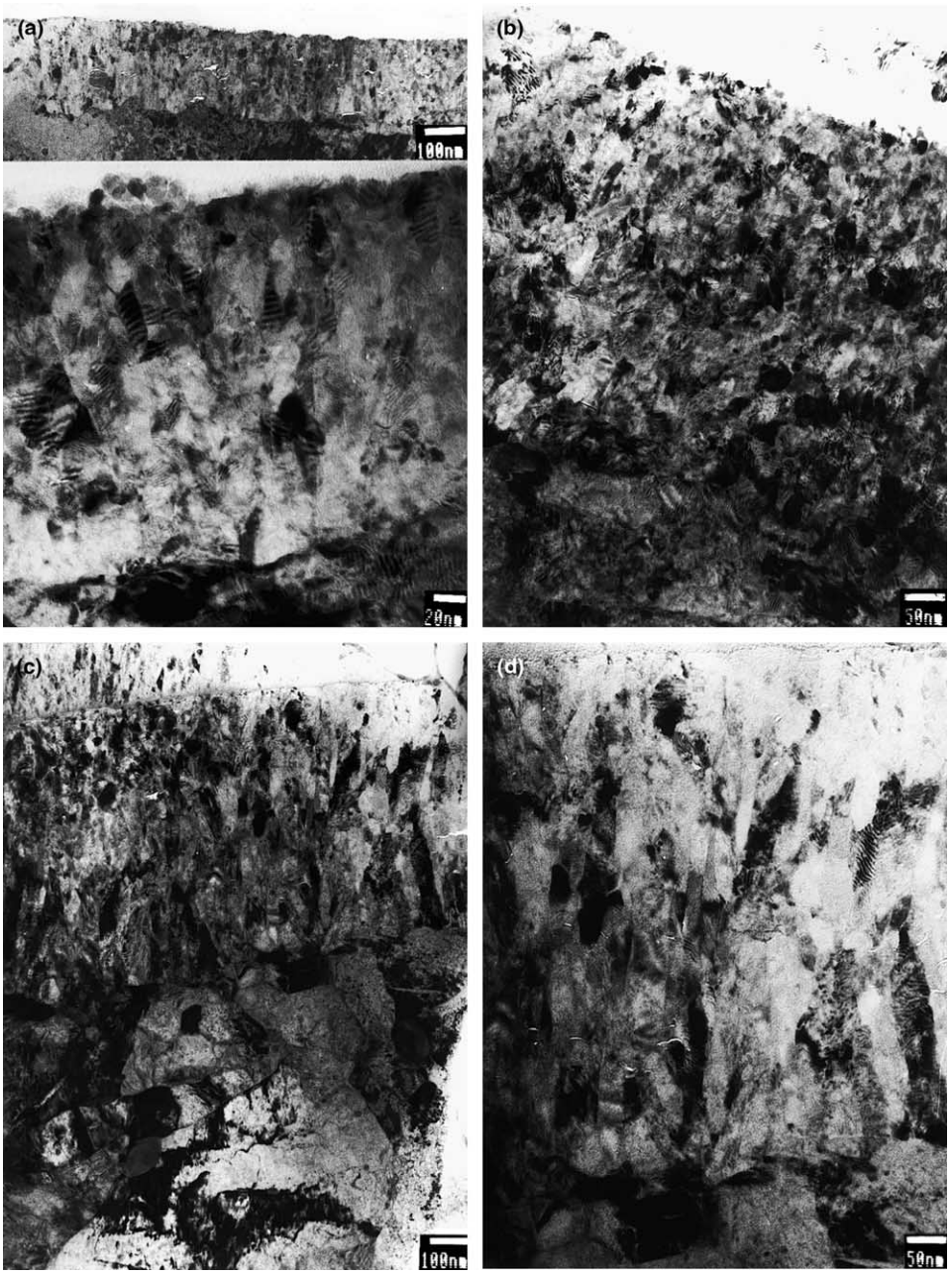

Fig. 2. TEM micrographs of sample Zry-2:A after oxidation at: (a) 288°C for 20 h. Overview at lower magnification in the upper part of the figure; (b) 288°C for 168 h; (c) 360°C for 96 h (overview); (d) 360°C for 96 h. At the top a thin layer of epoxy.

weight gain and TEM, Table 2, which indicates that the outer part of the oxide is macroporous. The fact that only a part of the oxide is accessible to impedance measurements is due to a low resistance over the outer part of the oxide as a result of the electrolyte penetration. The low resistance together with a small capacitance will yield a time constant that falls outside the accessible frequency range. To check if the oxide layer is porous the autoclaved sample was anodised by applying a voltage of 100 V. For an un-oxidised sample such an anodisation will yield an oxide thickness of about 300 nm. Thus, if the oxide layer on the autoclaved sample is compact the anodisation will have no effect on the oxide thickness. However, anodisation to 100 V results in a more compact oxide with a thickness in close agreement with the one expected from weight gain and TEM, Table

2. The reason for this is not fully understood, but the result shows that the resistance in the pores increases and it is thereby possible to measure the total oxide thickness. Also for the sample oxidised at 360°C for 96 h the outer part of the oxide is macroporous. In this case a second time constant is observed at high frequencies, but is not fully resolved and as a consequence the thickness of the layer cannot be obtained. After anodisation to 100 V the oxide thickness determined by impedance is in parity with the value obtained from weight gain and TEM.

4.2. Zry-2:B

The X-ray analysis for these three samples, see Fig. 3, are in accordance with the sample Zry-2:A. The sample oxidised for 168 h at 288°C has an oxide morphology with mainly columnar grains but also a fraction of equiaxed grains. The morphology of the oxide formed at shorter time is similar. The difference is that a few cracks, parallel with the interface are found in the thicker oxide layer, Fig. 4(a). The equiaxed grains are slightly larger at the longer exposure time. Oxidation at 360°C for 96h gave a morphology with longer columnar grains (comparable in size with sample Zry-2:A), Figs. 4(b) and 2(d).

The anodically formed oxide layer contains only equiaxed grains, with a diameter of 15–45 nm. The thickness of the formed oxide layer is ~300 nm as can be seen in Fig. 4(c). SAD analysis of this oxide showed the presence of monoclinic phase but also some tetragonal phase. The amount of tetragonal phase is larger in the anodically formed oxide compared to the thermally formed oxides and can readily be observed in X-ray diffraction, Fig. 5(a).

The impedance of the anodised sample shows the appearance of a compact film with only one time constant. The thickness is calculated to 300 nm, Fig. 5(b), in agreement with the results obtained by the TEM investigation, Fig. 4(c). Also for the thinnest autoclaved oxide, 288°C 20 h, a compact film is observed in the impedance diagram, Fig. 6(a), with slight frequency dispersion at low frequencies. The thickness calculated from the impedance data is in agreement with the value estimated from weight gain and TEM. When the oxide grows thicker at the same temperature, 288°C 168 h, a layered structure is formed as evident from the appearance of a second time constant at low frequencies, Fig. 6(b). As for sample Zry-2:A, the detectable thickness is lower than expected and the entire oxide layer can only be observed in the impedance measurements by anodising the sample. For the sample oxidised at 360°C for 96 h one time constant is observed, showing the compact nature of the oxide. The calculated thickness of the oxide layer is in agreement with the expected value, Fig. 6(c) and Table 2.

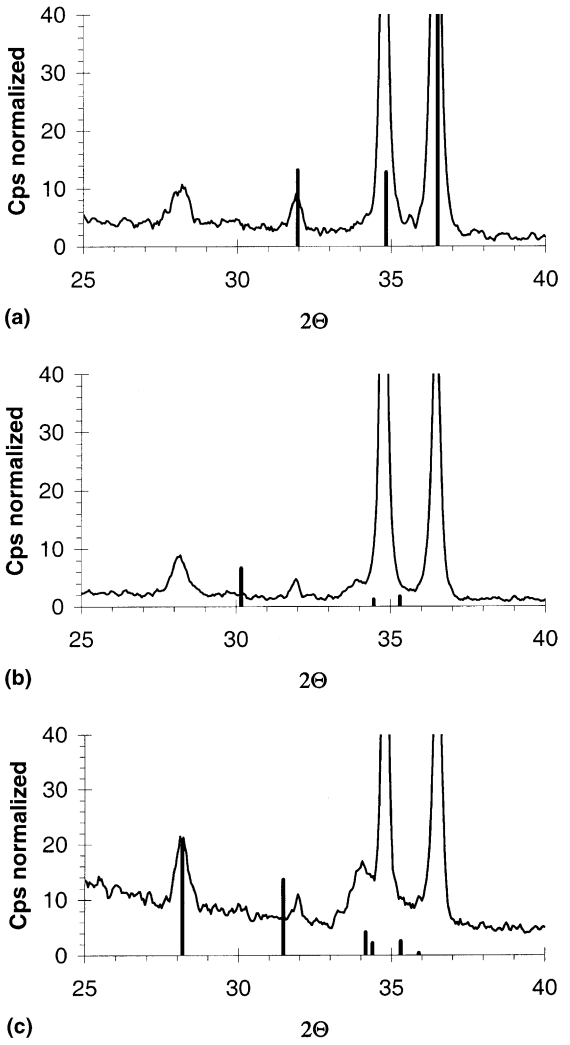

Fig. 3. X-ray diffraction analysis of sample Zry-2:B as a function of exposure time and temperature: (a) 288°C for 20 h; (b) 288°C for 168 h; (c) 360°C for 96 h. The standard reflection for Zr is given in (a), tetragonal ZrO_2 in (b) and monoclinic ZrO_2 in (c).

4.3. Zry-2:C

Sample Zry-2:C has the lowest weight gain of all studied samples. X-ray diffraction analysis and the TEM investigation of these samples are in agreement with the result from sample Zry-2:A. However, no tetragonal phase was discovered with SAD after the 20 h test. For this sample a layered structure was observed after the 360°C oxidation test, the outer part of the oxide layer contains less and shorter columnar grains, Fig. 7.

The impedance characteristics for this sample show that the oxide formed is rather compact. For the thinnest film one layer is observed, while for the thicker films

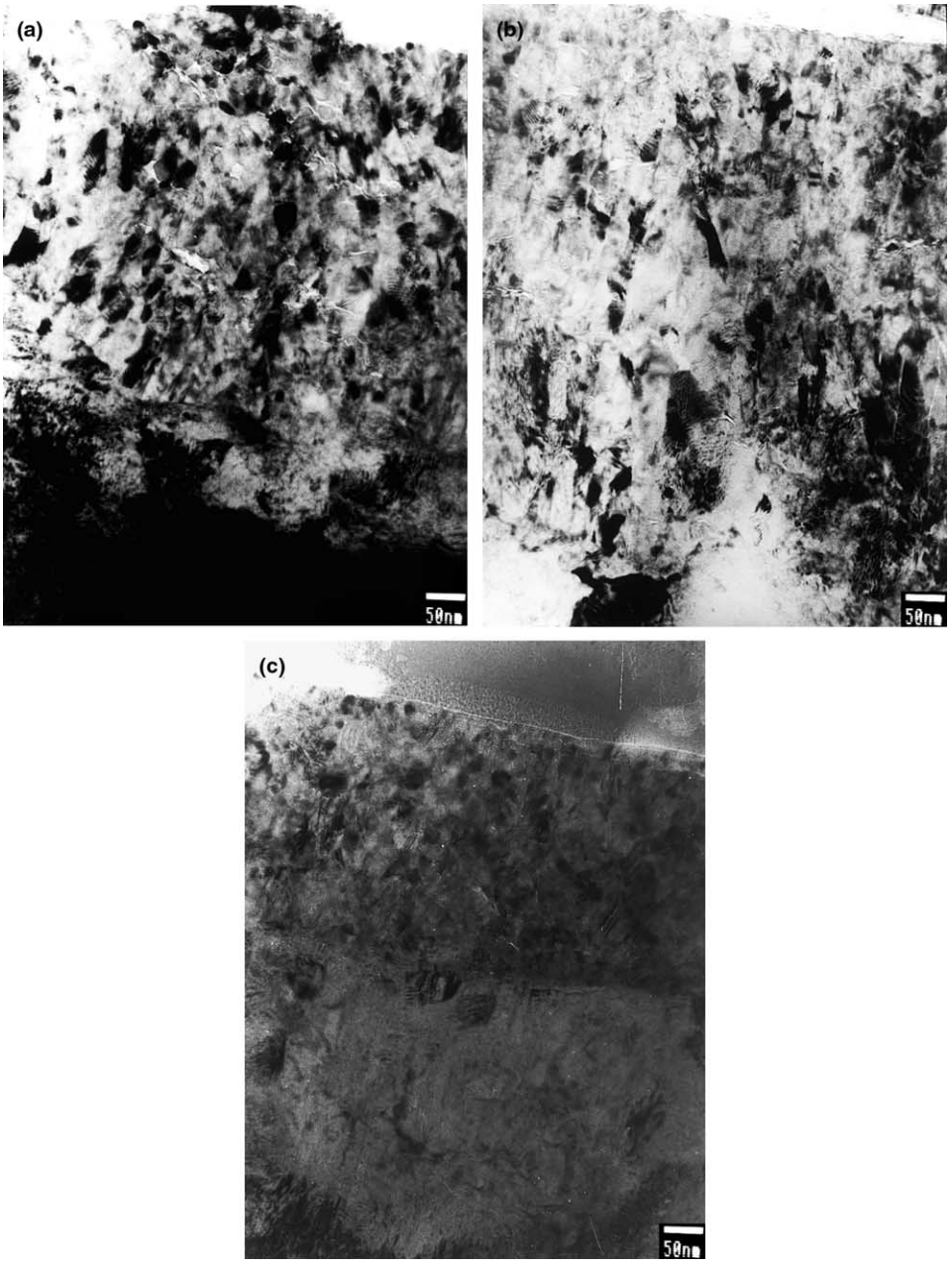

Fig. 4. TEM micrographs of sample Zry-2:B: (a) after oxidation at 288°C for 168 h; (b) after oxidation at 360°C for 96 h; (c) anodically formed oxide.

two layers are detected. However, for all three samples the oxide thickness determined from the impedance measurements is in agreement with the values obtained by weight gain and TEM, Table 2.

4.4. Zry-2:D

Sample Zry-2:D, oxidised for 20 h at 288°C, has the thickest oxide, compared to the four other investigated alloys (Table 2). Only monoclinic phase was found in X-ray diffraction analysis after the 288°C tests, while SAD shows presence of tetragonal/cubic phase after the 168-hour test. The morphology of the oxide formed at 288°C is similar to sample Zry-2:A. The higher oxidation temperature resulted also for this sample in a morphology with longer columnar grains and slightly larger equiaxed grains, Fig. 8. Some cracks in the grain boundaries were discovered in this sample.

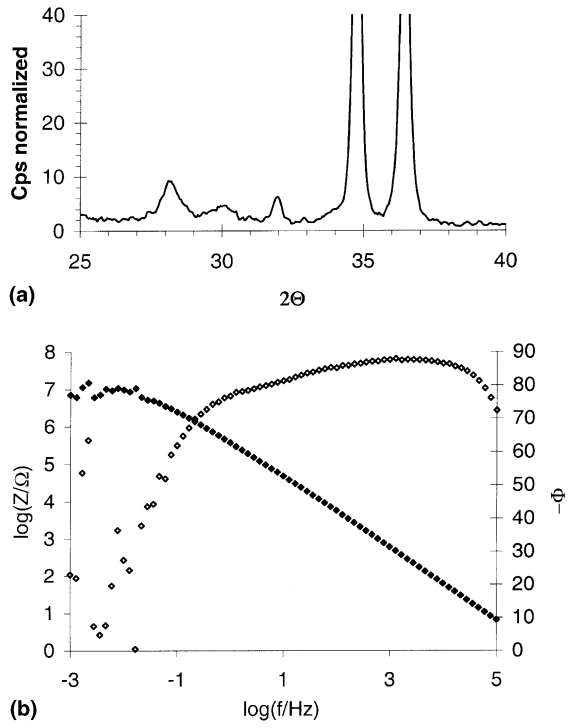

Fig. 5. Anodically formed oxide on sample Zry-2:B: (a) X-ray diffraction; (b) EIS.

A compact layer is observed for the two samples oxidised at 288°C and the thickness determined by impedance is in fairly good agreement with the values obtained from weight gain and TEM, Table 2. For the sample oxidised at 360°C for 96 h two time constants are observed, showing that the oxide is layered and the estimated thickness is slightly larger than expected from weight gain and TEM. In addition the resistance over the oxide is very low for this sample, which indicates that conductive paths are present.

4.5. Zry-4:A

Sample Zry-4:A is the only Zircaloy-4 variant studied. Only monoclinic zirconium dioxide was detected by X-ray diffraction in parity with the result on the Zircaloy-2 alloys, Fig. 9. The morphology, on the sample tested for 20 h at 288°C, has equiaxed (15–30 nm) and columnar grains (15–30 × 35–60 nm^2). After 168 h the oxide gets thicker and a slight increase of the grain size is found for the equiaxed grains. At the higher temperature (360°C) longer columnar grains were also observed on this sample and the maximum size for the equiaxed grains (20–50) is almost twice that found on samples tested at the lower temperature.

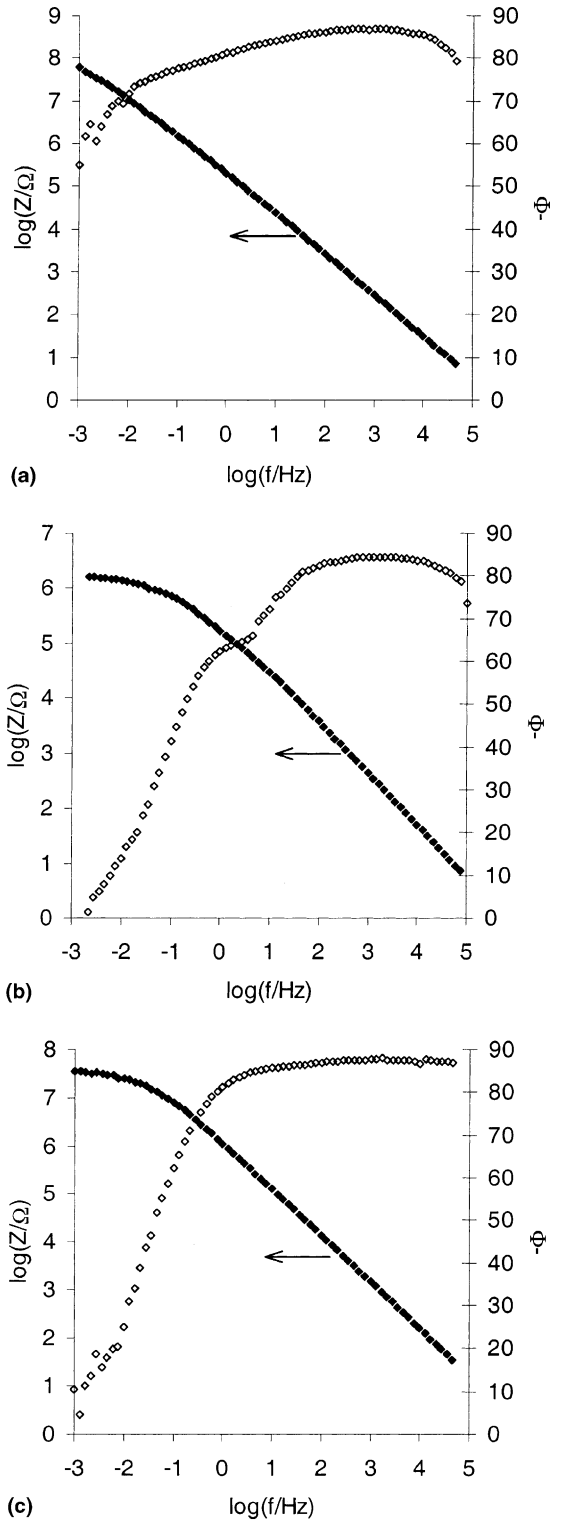

Fig. 6. EIS sample Zry-2:B as a function of exposure time and temperature: (a) 288°C for 20 h; (b) 288°C for 168 h; (c) 360°C for 96 h.

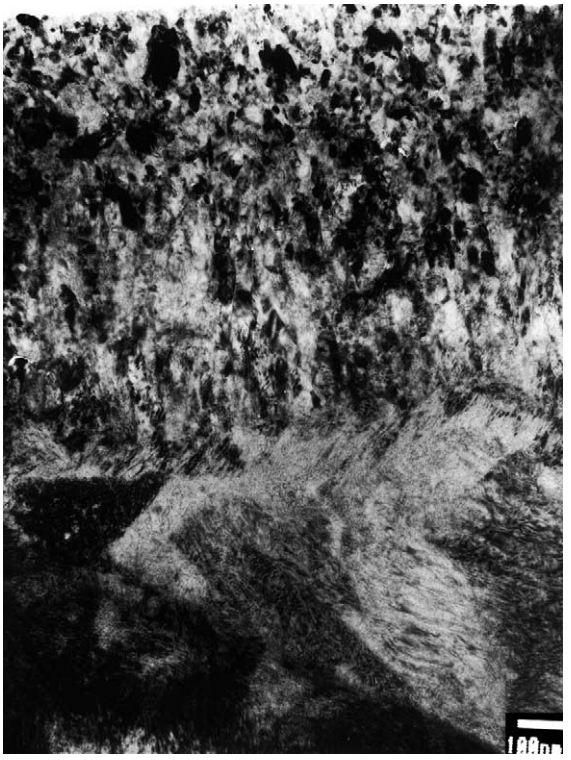

Fig. 7. TEM micrograph of sample Zry-2:C after oxidation at 360°C for 96 h.

Fig. 8. TEM micrograph of sample Zry-2:D after oxidation at 360°C for 96 h.

The impedance characteristics for this sample resemble that of sample Zry-2:A, with one layer for the thinnest film and with the development of a macroporous outer part at longer exposure times. For the sample oxidised at 360°C for 96 h, the oxide thickness cannot be determined because the resistance over the outer part of the oxide is low and the time constant falls outside the frequency range used. However, by anodising the autoclaved sample the entire oxide layer can be characterised, Table 2.

5. Discussion

In this study, differences in the pre-transition oxide were sought for that could be used to predict the post-transition oxidation kinetic. No major differences in the morphology and phase composition of the formed oxide layers were found between the different alloys. The impedance measurement shows that the oxide formed on alloys Zry-2:D, Zry-2:C and Zry-2:B is fairly dense, while for Zry-2:A and Zry-4:A the oxide formed at longer exposure times has a porous outer layer. The alloys with the more dense oxide layer appear to have better corrosion resistance in long time testing in water, Table 3. For the testing in lithiated water, Table 3 Zry-2:A seems to have the best corrosion resistance, while Zry-2:B has the highest corrosion rate. However, this cannot be explained by the impedance measurements. A reason might be that the alloys have different second phase particle distribution and size, which effect the microstructure (cracks and pores) in the post-transition region, but less in the pre-transition region. The accelerated corrosion commonly observed in the presence of lithium is mainly due to an up-concentration of the LiOH in cracks and pores [19] and it is, therefore, not surprising that no predictions can be made from measurements on pre-transition oxides.

A significant difference in morphology was found for the two test temperatures. Tests at the higher temperature resulted in larger oxide grains, especially the length of the columnar grains. The reason for the difference in morphology between the two temperatures is not fully understood but the results show that accelerated testing at elevated temperatures may be doubtful. A temperature change will cause differences of the oxygen partial pressure in water, the activity of oxygen in the metal, the diffusivity of oxygen ions, the driving force for oxidation and the nucleation of new oxide grains, amongst others.

The only difference between the two autoclave tests used in the present investigation is, besides the temperature, the pressure. At 288°C the equilibrium pres-

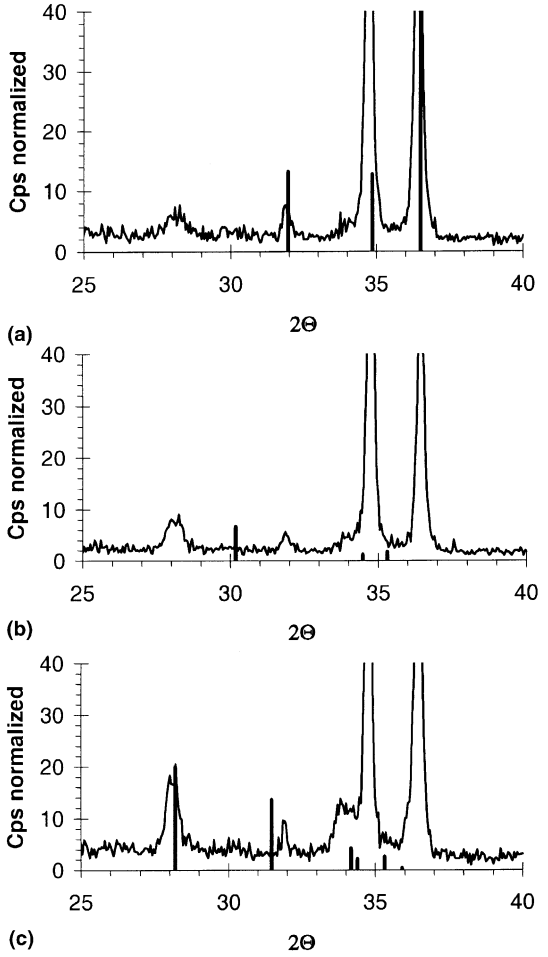

Fig. 9. X-ray diffraction analysis of sample Zry-4:A as a function of exposure time and temperature: (a) 288°C for 20 h; (b) 288°C for 168h; (c) 360°C for 96 h. The standard reflection for Zr is given in (a), tetragonal ZrO_2 in (b) and monoclinic ZrO_2 in (c).

sure is 72 bar and at 360°C 186 bar. The pressure was chosen so that water was present at both test temperatures. The pressure will affect the oxygen activity in water. However, since the oxidation rate is controlled by oxygen diffusion through the growing oxide [3], the oxygen activity in water is less important. Measurements at constant temperature (360°C) but different pressures (186 and 220 bar) show that the columnar grains are comparable in size [19]. Thus, the pressure cannot be the causing factor for the observed morphology difference.

The driving force for oxidation increases with temperature but since the oxidation is kinetically limited at both temperatures this factor is of minor importance. Instead, the oxidation rate is mainly determined by the diffusion rate of oxygen, which is exponentially dependent on temperature. The diffusion along grain boundaries is significantly faster than bulk diffusion. At the lower temperature a higher fraction of the oxygen originates from grain boundary diffusion and one possible explanation for the enhanced nucleation at this temperature may be a local increase in oxygen content in the metal close to the grain boundaries.

Since the yield strength of the metal is temperature dependent, one explanation for the difference in morphology between different temperatures could be that the new oxide grains are nucleated to decrease the compressive stress. A different crystal orientation is favourable to lower the stress. Plastic deformation of the metal is shown in numerical simulations where the stress distribution as a function of interface roughness is calculated [20]. However, the difference in yield strength is too low to explain the difference in morphology but it seems reasonable to decrease the compressive stress, new nuclei are formed.

5.1. Correlations between alloy composition, pre- and post-transition oxidation

The most important properties of the oxide layer during post-transition oxidation are the thickness and the passivating properties of the barrier layer. The oxidation rate is found to be dependent on distribution of second phase particles. Autoclave tests on Zircaloy-4 with small/medium or large second phase particles have shown that the corrosion rate is dependent on the size distribution of second phase particles [7], i.e., the particles should not be too small or too large. The mechanism by which intermetallic particles affect the oxidation behaviour for Zircaloy may be a mechanical effect. The movement of the phase interface (α-Zr to ZrO_2) may be slowed down when particles with a different crystallographic structure are present in the metal phase. The particles act as obstacles for the moving interface and the maximum effect is when the particles have an optimal size and are lying close enough to each other. Due to the slower oxidation of the second phase particles compared to the matrix, large particles will act as 'electronic bridges' throw the oxide layer. The oxidation rate is also reported to be dependent on the chemical composition of the intermetallic precipitates [21]. However, since zirconium has a very high affinity for oxygen, the oxidation rate in the pre-transition region is not affected by the presence of other elements.

5.2. Comparison between anodically and thermally formed oxides

Anodic oxidation has been used to produce oxide films on Zircaloy for many years. The sample is put in an aqueous electrolyte and an electrical field is applied between the zirconium anode and a platinum cathode.

One study reports that the oxide films produced in different aqueous electrolytes are generally characterised by randomly orientated equiaxed oxide grains (diameter 45–50 nm) and with cubic phase [22]. Incorporation of anions from the electrolyte may influence the oxide morphology and the incorporation increases with current density. In 0.1 M H_2SO_4 solution up to 0.1 anion per molecule ZrO_2 has been reported to be built in [23]. During anodic oxidation oxygen ions are suggested to be the moving species [24], but also cation transport is reported [25].

In the present study it is shown that the formed oxide layer is composed of randomly orientated equiaxed grains with mainly monoclinic zirconium oxide. However, a detectable amount of the tetragonal zirconium oxide is also observed in X-ray diffraction, Fig. 5(a). This can be compared to thermally formed oxide layers, which are characterised by mainly columnar oxide grains, and where the grains have a texture, i.e., growth direction perpendicular to the metal/oxide interface. For the thermally formed oxides the existence of tetragonal phase could only be proved in the TEM investigation, which indicates that the fraction tetragonal phase is low. EIS measurement on the anodically formed oxide show a compact oxide layer, in agreement with the results found on thermally formed oxide layers at the same thickness.

SAD was used to investigate if tetragonal/cubic phase is present in the oxide. In this study only small amounts of tetragonal phase were detected in the oxide layer. As discussed elsewhere [26] the TEM sample preparation is suggested to influence the presence of the high temperature phases. Since the tetragonal/cubic phases are stabilised by stress and the relaxation during preparation may explain why only small amounts of these phases are found in TEM despite the fact that they may be present during oxide growth. Based on a study of the oxide layers with Raman spectroscopy [7], where it is reported that the oxide layer closest to the metal/oxide interface contains as much as 40% tetragonal phase, the stress relief of the oxide layer was proposed to decrease the amount of tetragonal oxide. However, in the present study the high temperature phase is mainly observed in the SAD study, while the amount of the tetragonal phase in the thermally formed oxides is too low to be detected by X-ray diffraction. Thus, the tetragonal phase is probably stabilised by other factors than the compressive stress, in accordance with [27].

6. Conclusions

Five different zirconium alloys have been tested in autoclave at 288°C for 20 h and 168 h and at 360°C for 96 h. The pre-transition oxides are characterised by cross-sectional TEM, X-ray diffraction analysis and Electrochemical Impedance Spectroscopy and the results from the investigations are:

- Main differences in morphology were found between the two test temperatures, while the alloy composition was found to have no influence. At the higher temperature (360°C) the size of the columnar grains increases a factor 3–4 in length compared to the oxide formed at 288°C.
- At 288°C the oxide consists of a mixture of columnar and equiaxed grains, but at 360°C mainly columnar grains are observed.
- The tetragonal oxide phase was only detected by selected area diffraction in the thicker oxide layers, since the amount of the tetragonal phase in the thermally formed oxides is too low to be detected by X-ray diffraction. Thus, the tetragonal phase is probably stabilised by other factors than the compressive stress.
- The impedance measurement shows that the oxide formed on alloys Zry-2:D, Zry-2:C and Zry-2:B is fairly dense, while for Zry-2:A and Zry-4:A the oxide formed at longer exposure times has a porous outer layer.
- One sample, Zry-2:B, was also anodically oxidised. The formed oxide layer has only equiaxed grains present and both tetragonal and monoclinic phases were identified in SAD as well as in X-ray diffraction.

The aim of this study was to evaluate the possibility of predicting post-transition oxidation behaviour by studying the properties of pre-transition oxides. Based on the result obtained in this investigation, no such prediction can be made.

Acknowledgements

Financial support from the Swedish Nuclear Power Inspectorate (SKi) is gratefully acknowledged. This work was carried out as a part of the Swedish research programme for the understanding of Zircaloy corrosion and hydriding mechanisms, funded by ABB Atom AB, Barsebäck Kraft AB, OKG AB, and Vattenfall. ABB Atom AB is also gratefully acknowledged for the supply of tested tubes.

References

[1] Y. Hatano, M. Sugisaki, J. Nucl. Sci. Technol. 33 (1996) 829.
[2] R.L. Tapping, J. Nucl. Mater. 107 (1982) 373.
[3] B. Cox, C. Roy, Electrochem. Technol. 4 (1966) 121.
[4] A. Grandjean, Y. Serruys, J. Nucl. Mater. 273 (1999) 111.
[5] G.P. Sabol, S.G. McDonald, G.P. Airey (Eds.), Microstructure of the Oxide Films Formed on Zirconium-Based Alloys, vol. ASTM STP 551, 1974.
[6] B. Cox, J.P. Pemsler, J. Nucl. Mater. 28 (1968) 73.

[7] J. Godlewski, J.P. Gros, M. Lambertin, J.F. Wadier, H. Weidinger, in: C.M. Eucken and A.M. Garde (Eds.), Zirconium in the Nuclear Industry, 9th International Symposium, vol. ASTM STP 1132, Kobe, Japan, 1991, p. 416.
[8] B.D. Gelas, G. Beranger, P. Lacombe, J. Nucl. Mater. 28 (1968) 185.
[9] J. Godlewski, in: A.M. Garde, E.R. Bradley (Eds.), Zirconium in the Nuclear Industry, 10th International Symposium, vol. ASTM STP 1245, Baltimore, MD, 1994, p. 663.
[10] J.N. Wanklyn, Corrosion of Zirconium Alloys ASTM STP368 (1964) 58.
[11] T. Kido, in: R.E. Gold, E.P. Simonen (Eds.), Sixth International Symposium on Environmental Degradation of Materials in Nuclear Power System-Water Reactors, San Diego, CA, 1993, p. MMMS 449.
[12] A.M. Garde, in: C.M. Eucken, A.M. Garde (Eds.), Zirconium in the Nuclear Industry, 9th International Symposium, vol. ASTM STP 1132 Kobe, Japan, 1991, p. 566.
[13] M. Blat, D. Noel, in: E.R. Bradley, G.P.Sabol (Eds.), Zirconium in the Nuclear Industry, 11th International Symposium, vol. ASTM STP 1295, Garmisch-Partenkirchen, Germany, 1996, p. 319.
[14] M. Blat, L. Legras, D. Noel, H. Amanrich, in: G.P. Sabol, G.D. Moan (Eds.), Zirconium in the Nuclear Industry: 12th International Symposium, vol. ASTM STP 1354, Toronto, Canada, 2000, p. 563.
[15] M. Oskarsson, E. Ahlberg, U. Södervall, U. Andersson, K. Pettersson, J. Nucl. Mater. 289 (2001) 315.
[16] H.-U. Zwicky, H. Loner, B. Andersson, C.-G. Wiktor, J. Harbottle, in: ANS International Topical Meeting on Light Water Reactor Fuel Performance, Park City, UT, 2000.
[17] J. Jacquelin, Electrochim. Acta 39 (1994) 2673.
[18] G. Paasch, K. Micka, P. Gersdorf, Electrochim. Acta 38 (1993) 2653.
[19] M. Oskarsson, E. Ahlberg, K. Pettersson, J. Nucl. Mater. 295 (2001) 97.
[20] M. Parise, O. Sicardy, G. Cailletaud, J. Nucl. Mater. 256 (1998) 35.
[21] D. Charquet, in: G.P. Sabol, G.D. Moan (Eds.), Zirconium in the Nuclear Industry, 12th International Symposium, vol. ASTM STP 1354, Toronto, Canada, 2000, p. 3.
[22] R.A. Ploc, M.A. Miller, J. Nucl. Mater. 28 (1971) 71.
[23] C. Ortega, J. Siejka, J. Electrochem. Soc. 129 (1982) 1905.
[24] J.S. Whitton, J. Electrochem. Soc. 115 (1968) 58.
[25] N. Khalil, A. Bowen, J.S. Leach, Electrochim. Acta 33 (1988) 1721.
[26] F. Garzarolli, H. Seidel, R. Tricot, J.P. Gros, in: C.M. Eucken, A.M. Garde (Eds.), Zirconium in the Nuclear Industry: 9th International Symposium, vol. ASTM STP 1132, Kobe, Japan, 1991, p. 395.
[27] N. Petigny, P. Barberis, C. Lemaignan, C. Valot, M. Lallemant, J. Nucl. Mater. 280 (2000) 318.